Novel simulation technique for efficient fabrication of 2m class hexagonal segments for extremely large telescope primary mirrors

Dae Wook Kim*[a], Sug-Whan Kim[abc]

[a]Space Optics Laboratory, Department of Astronomy, Yonsei University, Republic of Korea
[b]Institute of Space Science and Technology, Yonsei University, Republic of Korea
[c]Center for Space Astrophysics, Yonsei University, Republic of Korea

ABSTRACT

2m class hexagonal primary mirror segments for extremely large telescopes such as OWL and EURO50 receive an increased attention from the optics fabrication community world-wide. We report the development of a novel simulation technique offering cost-effective mass fabrication strategies for such mirrors of tight specifications. A family of static tool influence functions (TIFs) was derived using the Preston's material removal equation. We then confirmed that the mathematical TIFs can re-produce the material removal foot prints of the bulged precessing tooling reported elsewhere. For fabrication simulation, these TIFs are fed into the in-house developed polishing algorithm that uses a combination of the fixed tool path patterns and the floating trajectory management based on the error grid weighting and the irregular tool paths. The algorithm also optimizes other control parameters including dwell time and tool pressure in real-time as the machine runs. Trial simulation runs using various combinations of the TIFs and the polishing algorithm showed the feasibility of producing the 2m class primary segments with the bulged precessing tooling. The details of the simulation technique together with the results and implications for mass fabrication are presented.

Key-words: Extremely large telescope, Hexagonal segments, Bulged precessing tool, Tool influence function, Polishing algorithm, Fabrication simulation

1. INTRODUCTION

1.1. Specifications for the recent ELTs

The Extremely Large Telescopes (ELTs), currently being planned, have hexagonal, segmented primary mirrors of about 1-2 m in diameter.[1] As shown in Table 1, the target specifications of these ELTs primary mirrors are highly challenging. Examples may include the EURO50 primary segment that is to have the peak to valley form accuracy of less than 18nm that is equivalent to less than 1/30 wavelength.[2] The continuing change in slope difference between the target shape and the best fit sphere serves as the primary cause to the fabrication difficulty in the case of conic surface fabrication.[3] The difficulty criterion dy in Table 1 can be estimated with

$$dy = \frac{8 \cdot (f / D)^3}{k} \tag{1}$$

,where k is the conic constant of the primary mirror, f the focal length, and D the diameter of the primary mirror. The dy for each telescope, except for OWL that has a spherical primary, is presented in Table 1. It shows that, even without considering mass fabrication requirement, the EURO50 primary segment (dy=4.92) is about 5.3 times more difficult than the KECK primary segment (dy=26.1.)

For this reason, the classical fabrication methods available before 1985, whilst being capable of producing the final surfaces of typically more than 80nm rms accuracy, can not deliver the ELT segments on time and on budget.[3] More recent polishing techniques, of course, result in much better surface rms accuracy. For instance, the ion beam figuring technique was extensively used to successfully fabricate the 36 hexagonal mirror segments of the KECK telescope that

Optical Design and Testing II, edited by Yongtian Wang, Zhicheng Weng, Shenghua Ye, José M. Sasián, Proc. of SPIE Vol. 5638
(SPIE, Bellingham, WA, 2005) · 0277-786X/05/$15 · doi: 10.1117/12.576702

has the typical rms accuracy of 15nm.[3] However, the technique has the extremely low material removal rate and consequently suffer from the long delivery schedule. A study indicated that the ion figuring method would take about 8 years to complete the 1080 of CELT segments with 6 figuring chambers.[4] This does not even include the requirement of a number of the precision grinding and pre-polishing machines for producing the input mirror surfaces of sub-micron accuracy to the ion figuring machines. This demonstrates the critical limitation of its applicability to the mass fabrication requirement in the order of few hundreds and even thousand units of the ELT primary mirror segment.

Table-1. Specifications of the ELTs and KECK primary mirrors

	Primary Mirror Diameter (m)	F-ratio of Primary Mirror	Segment Size (m)	Conic Constant	# of Segments	dy	Segment Shape
EURO50	50.4	f/0.85	2	-0.9994	618	4.92	Hexagonal
OWL	100	f/1.82 or f/1.5	1.6	0	3048	n/a	Hexagonal
CELT	30	f/1.50	0.5	-1.525	1080	17.7	Hexagonal
KECK	10	f/1.75	1.8	-1.644	36	26.1	Hexagonal

1.2. New development of mass fabrication method

Among many, three process elements are crucial for the successful deployment of efficient mass fabrication technique for the large, precision segmented mirrors. They are i) low tooling overhead, ii) deterministic material removal and iii) embedded process control intelligence. The recent introduction of Zeeko's IRP series machines employing the Precessions™ process offers much greater improvement in all three elements defined above.[2] In particular, the process uses a family of bulged precessing tools that tends to conform its shape to the local surface, and that variable size tool-surface contact area is achieved with a single bonnet. Such tooling ability aided with a precision 7 axis CNC capability (including workpiece rotation) and the built-in Precessions™ process intelligence demonstrated a moderate success in deterministic form control ability for the circularly symmetric workpieces.[2]

However, this process, as is of today, cannot be directly applicable to the ELT primary mirror segments because of their aspheric profiles and the hexagonal shape. The production is further complicated with the mass fabrication requirement within the reasonable delivery time of 2-3 years. This gives rise to the need of the new fabrication technique that adds the axially non-symmetric workpiece capability and even higher deterministic process control ability to the existing bulged precessing tool process. To this extent, the present technical development, reported here, forms an attractive solution to the challenging problems of mass fabrication of segmented mirrors for the ELT projects. Chapter 2 deals with the theoretical background of tool influence function used in the existing precessing polishing and the experimental verification. This is followed by the explanation of polishing algorithm in Chapter 3. The simulated polishing results for three surface error cases and its scaling interpretation for the mass fabrication are presented in Chapter 4. Chapter 5 summarizes the implications.

2. TIF GENERATION AND VERIFICATION

2.1. Theoretical tool influence functions (TIFs)

The equation of material removal (EMR) is derived from the well-known Preston's relation that the material removal from the workpiece surface is proportional to applied pressure, velocity, and dwell time. The Preston's equation is written as

$$\Delta z = \kappa \cdot P \cdot V_T \cdot \Delta t \tag{2}$$

, where κ is the removal coefficient of the segment, P polishing pressure, V_T magnitude of relative speed between the tool and workpiece surface, and Δz the material removal from the workpiece surface .

As shown in Figure 1, the Gaussian pressure distribution inside the tool-workpiece contact area of the bulged precessing tool is used in the Precessing[TM] polishing. Its mathematical representation can be written as a modified Gaussian function with standard deviation σ and maximum value P_T,

$$P = P_T \cdot (e^{-\frac{\lambda^2}{2\sigma^2}})^{\psi} \quad (3)$$

, where λ is the distance between A and C, and ψ the modification constant of Gaussian pressure distribution. For non-rotating hexagonal segment surfaces, the total velocity V_T is the vector sum of tool rotation V_{TR} and the feed rate V_{TF}. This can be expressed as the equation below.

$$V_T = \sqrt{(V_{TRx} + V_{TFx})^2 + (V_{TRy} + V_{TFy})^2} \quad (4)$$

Replacing P and V_T of equation 2 with equation 3 and 4, hence EMR is written as equation 5.

$$\Delta z = \kappa \cdot P_T \cdot (e^{-\frac{\lambda^2}{2\sigma^2}})^{\psi} \cdot \sqrt{(V_{TRx} + V_{TFx})^2 + (V_{TRy} + V_{TFy})^2} \cdot \Delta t \quad (5)$$

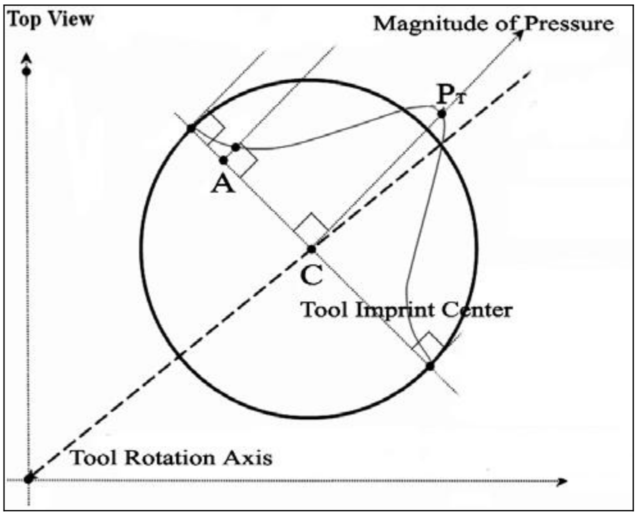

Figure-1 Gaussian-like pressure distribution

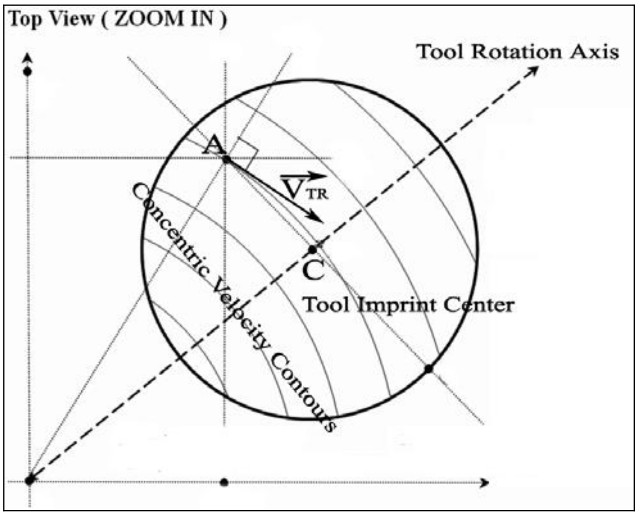

Figure-2. Concentric, traditional, velocity contours

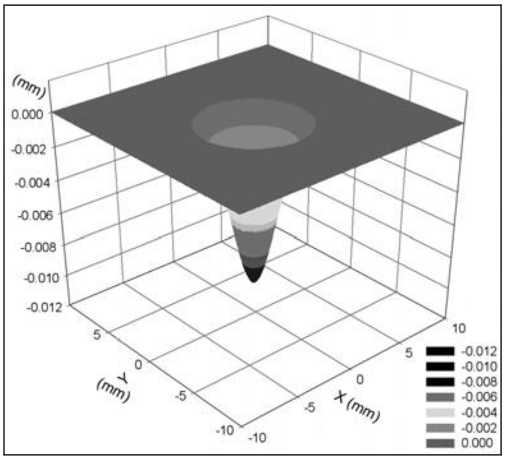

Figure-3. Computer generated TIF (3D-view)
(Δt=6 sec, W_T=1000rpm, P_T=0.013Mpa, α=15deg)

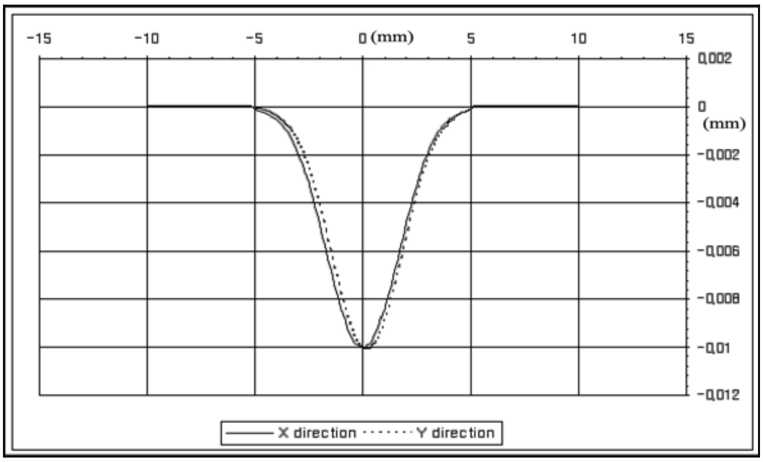

Figure-4. Sectioned profiles of the TIF in X and Y axis

When the equation 5 is applied with a set of polishing machine and workpiece parameters, static TIF can be produced as shown in Figure 3 and 4. For example, when the workpiece attack (i.e. inclination) angle of 15 degree and the fixed precession angle of 0 degree as well as other conditions expressed in Figure 3 were used, a 3D TIF (Figure 3) and its 2D sectional profiles (Figure 4) were obtained. Here we note the shape difference between the X- and Y-sectional profiles of the TIF, this being caused by the un-symmetric velocity field effect with the fixed precessing angle as depicted in Figure 2. The asymmetric tool velocity field is strongly tied with changes in precessing angle. This leads to at least 3-4 precessing angles to be used for generation of a circularly symmetric Gaussian looking TIFs.

2.2. Experimental verification of TIFs

The theoretical TIFs were verified against the characteristics of the measured TIFs[5, 6] obtained with different combination of tool rpm (W_T), inclination angle (α) and tool pressure (P_T). First, a family of 10 theoretical TIFs generated with the tool rotation range of 100-1000 rpm, but with other parameters fixed, is shown in Figure 5. The TIF depth variation with the tool rotation shown in Figure 6 demonstrates that the linearity between the material removal depth and the tool rotation, observed experimentally[6], was reproduced at high precision. This implies that the material removal controllability can be achieved, both in simulation and in actual polishing, by altering the tool rotation.

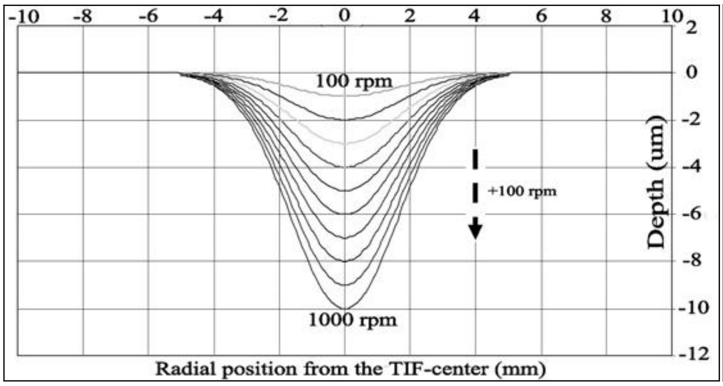

Figure-5. Computer generated TIFs (100~1000 tool rpm)

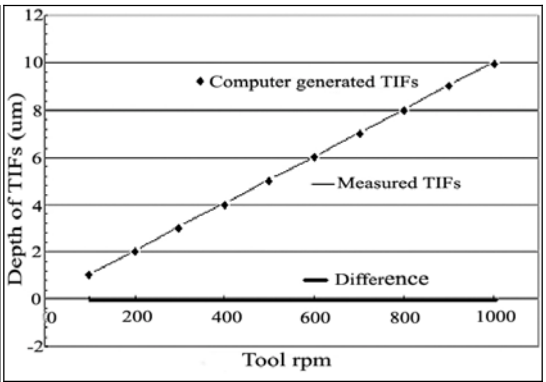

Figure-6. Depth of measured[6] and computer generated TIFs, and differences

Second, we then tested the effects of workpiece attack (i.e. inclination) angle onto the theoretical TIFs. When the inclination was changed from 6 to 20 deg, the TIFs showed the increased material removal depth, thought not as linear as with the tool rotation. Once again, Figure 8 shows that the theoretical TIFs follow the measurement[5] very closely. Whilst the theoretical and experimental plots show the difference of about 30nm for the inclination range of 14-18 degree, the material removal depth increases with the inclination.

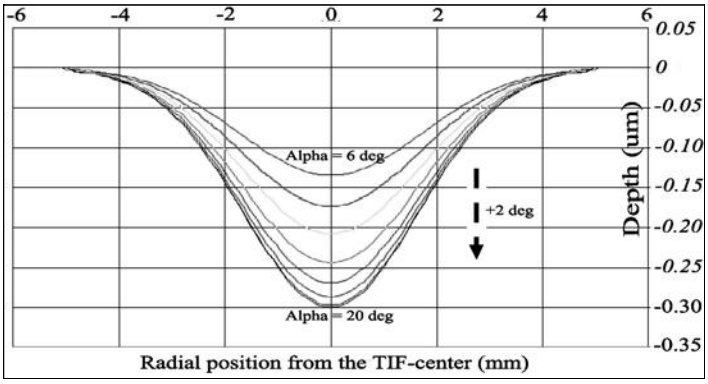

Figure-7. Computer generated TIFs (α: 6 ~ 20 deg)

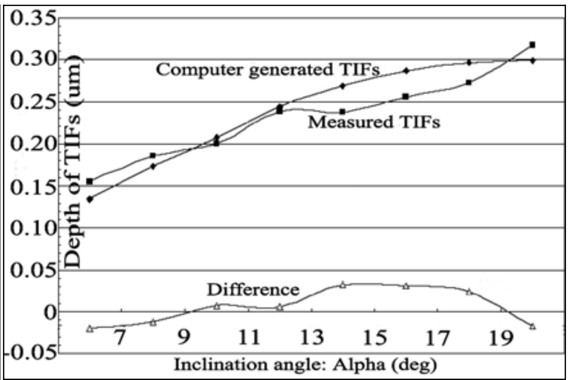

Figure-8. Depth of measured[5] and computer generated TIFs, and differences

Third, we generated a family of theoretical TIFs with the tool pressure ranging from 0.0130 Mpa to 0.0214 Mpa and other control parameters fixed. The measured[6] and computer generated TIFs are presented in Figure 9. Because the tool imprint radius, R_{TI}, and the depth of TIF are a function of the tool pressure, Figure 9 shows that the tool imprint radius increases from 5 mm to 7 mm and the depth of TIF from 3.6 um to 6 um. We note that the depth of TIF becomes 1.66 (=6/3.6) times higher, when R_{TI} increases by the factor of 1.4 (=7/5) times, showing a non-linear relationship. Nevertheless, the measured material removal depth and tool imprint radius were well reproduced with the theoretical TIFs. The minor difference in the width of the Gaussian profiles between both theoretical and experimental TIFs can be easily removed by adjusting the parameters of the Gaussian function in equation 3.

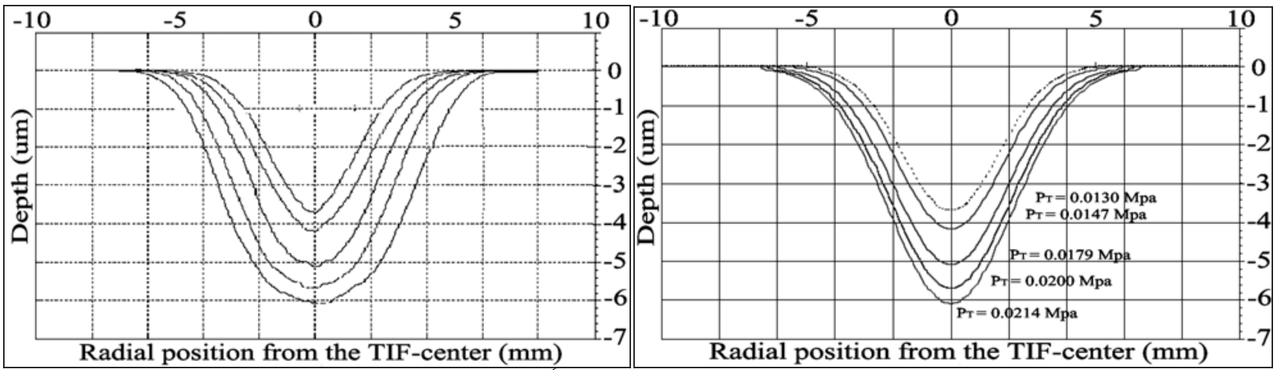

Figure-9. Measured TIFs[6] (left) and computer generated TIFs (right)

3. POLISING SIMULATION STRATEGY

3.1. Simulation control algorithm

The reproducibility of the experimental TIFs demonstrated above provided the theoretical material removal mechanism that can be used for the polishing simulation. The overall process flow for the machine control algorithm is given in Figure 10.

First, it takes the inputs of the initial set of polishing control parameters (i.e. P_T, W_T, Δt) and the given initial surface form error. Using these initial parameters, the process selects a fixed tool path first and then initiates the selected tool path motion. At this stage, three fixed tool path patterns, depicted in Figure 11 (top), are available in our simulation code. The tool path resolution is defined as the number of tool path lines, as seen in Figure 11 (bottom), in x and y directions. A relevant tool path resolution is calculated based on the tool imprint radius so that the entire workpiece surface is covered with the polishing action. This linear grid based tool path varies during the simulation process by the floating trajectory management that modulates the tool path resolution actively. In addition, residual material peaks left over from the combination of the fixed and floating grid based tool paths are efficiently removed by the irregular tool motion with relevant spot sizes.

The three process rules are applied for each and every tool-workpiece surface contact so that it protect the surface form from the excessive material removal due to the over-polishing, as follows.

- Rule 1: The PV form accuracy of the workpiece must be decreased in the course of fabrication process.
- Rule 2: The rms surface accuracy of the workpiece must be decreased in the course of polishing process.
- Rule 3: The maximum material removal depth tolerance is to be the half of the target PV form accuracy from the target workpiece surface.

These rules are to be strictly observed so that any possible violations would be avoided in the first place and, if un-avoidable, cause the termination of the simulation process. In addition, the dwell time for every tool-surface contact is estimated based on the residual surface error and other control parameters including tool pressure and spot size.

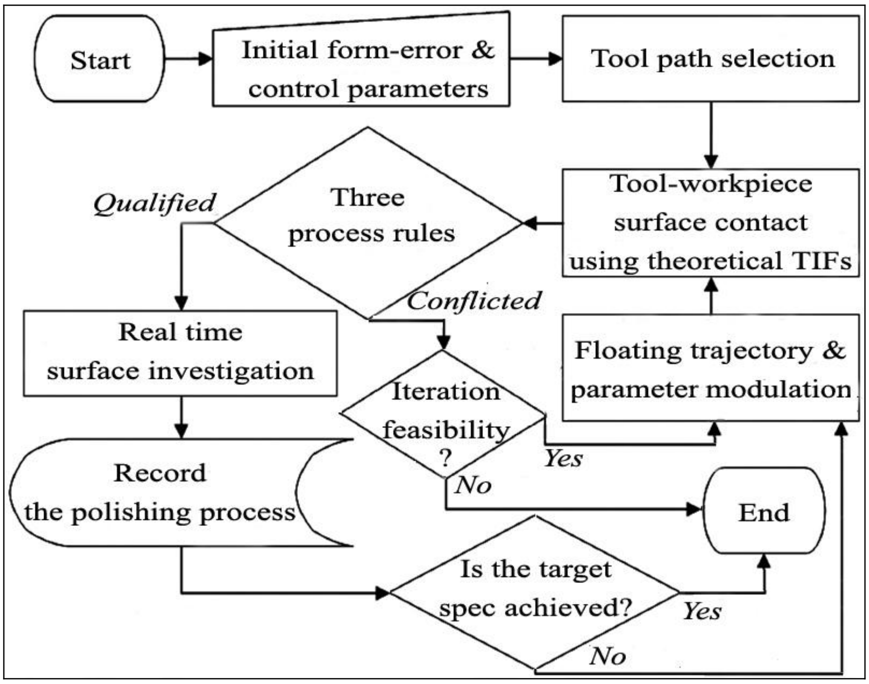

Figure-10. Polishing simulation process flow

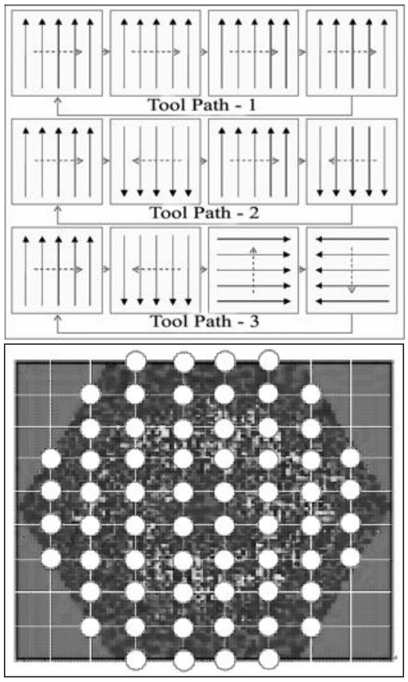

Figure-11. Three kinds of tool paths <top>
10 X 10 tool path resolution <bottom>
(white line: tool path, white circle: tool position)

4. RESULTS AND ANALYSIS

4.1. Simulation results

The polishing simulations were performed for the three different cases of initial form error of about 2um PV in depth. These errors have the shapes of bulged-center, donut-like, and circularly non-symmetric donut. The simulation code has no inherent numerical limitation regarding the target PV accuracy. However, the trial polishing simulations here used the target PV form accuracy of 60nm (~1/10 wavelength) for efficient demonstration of the simulation technique. The examples of some key simulation parameters, which may vary according to specific bulged precessing settings, are presented in Table 2.

Table-2. Bulged precessing tool characteristics

• Input parameters (60nm target PV form accuracy case)			
Tool Radius	R_T *(mm)*	400	
Removal Coefficient of the Segment[7]	κ *(Mpa^{-1})*	5.57*10^(-7)	BK7
Inclination Angle	α *(deg)*	15	
Precession Angles in one 'tool-workpiece surface contact'	δ *(deg)*	0, 120, 240	

4.1.1. Case-I: Bulged-center

The symmetric 'bulged-center' initial form error of the PV form accuracy of 2 microns has the prominent form deviation from the best fitting sphere concentrated at around the workpiece center. The initial segment surface is depicted in Figure 12 (left) and the final simulation results in Figure 12 (right). The history of various control parameters such as tool pressure, spot size, tool rpm, and so on, plotted into various control parameter graphs in Figure 13.

We note 10 irregular tool motions invoked during the simulation, resulting in rapid decreases of the form accuracy and the contact spot size in Figure 13. The close link between the reduction of the spot size and the rapid form improvement is clearly demonstrated, as shown in the shaded zones in Figure 13. The net fabrication time (i.e. integrated dwell time expressed as elapsed time in Figure 12) was about 3 hours (190.4 minutes) for the case-I, for which 5078 tool-workpiece surface contacts were made and 98% of the initial surface errors removed both in PV and rms. The final surface errors reached the PV form accuracy of 49nm PV and the rms surface error of 10nm rms.

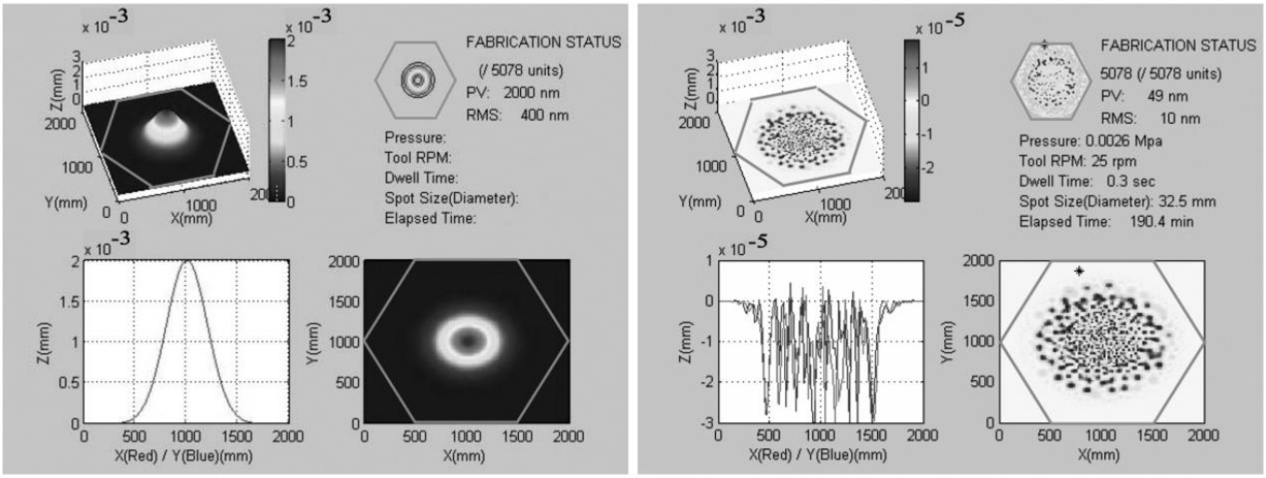

Figure-12. Initial (left) and final (right) surface status for the bulged-center case

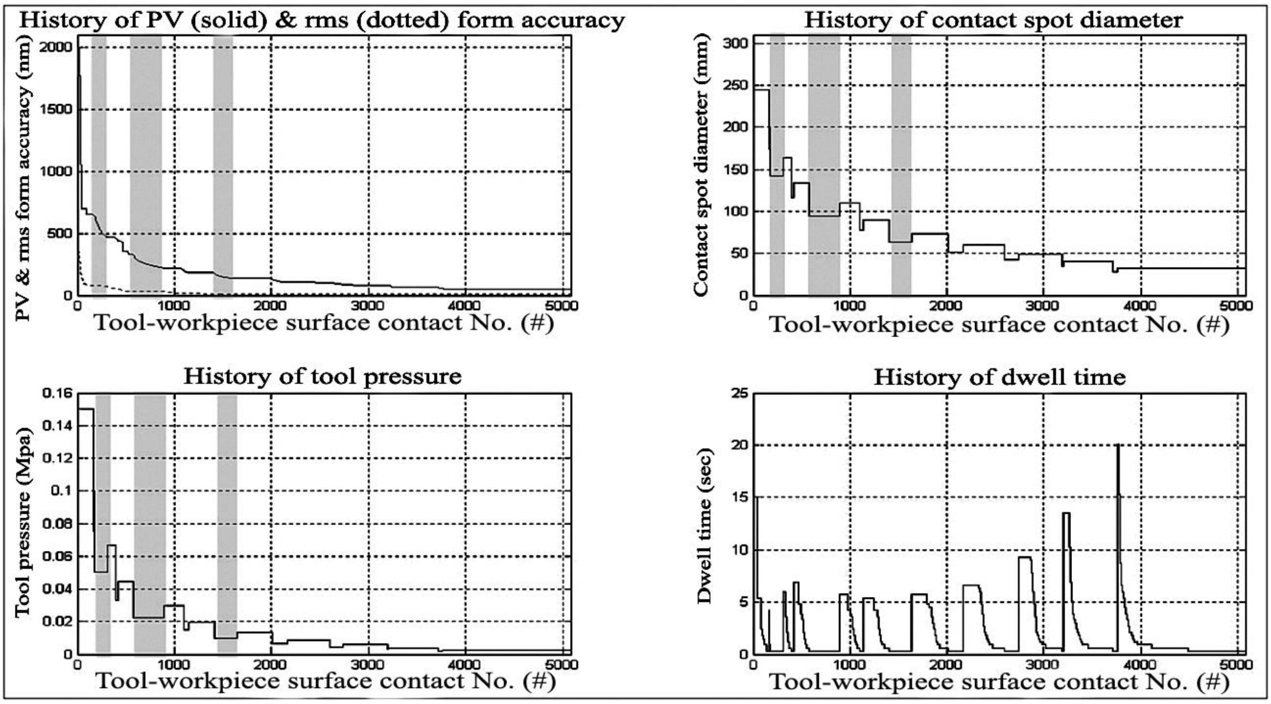

Figure-13. Evolution of control & surface parameters (bulged-center case)

4.1.2. Case-II: Donut-like

The symmetric 'donut-like' initial form error has the input PV form accuracy of 1.983 microns, but the initial rms is about 3 (=1211/400) times of the case-I. The initial and the final surfaces are drawn in Figure 14. The major difference in net fabrication time between case-I and II is caused by the case-II initial form error spread out over a wider area than case-I and by the smaller residual patterns on the segment remained until the final stage of the fabrication. The simulation resulted in the PV form accuracy of 59nm PV and the rms form accuracy of 15 nm.

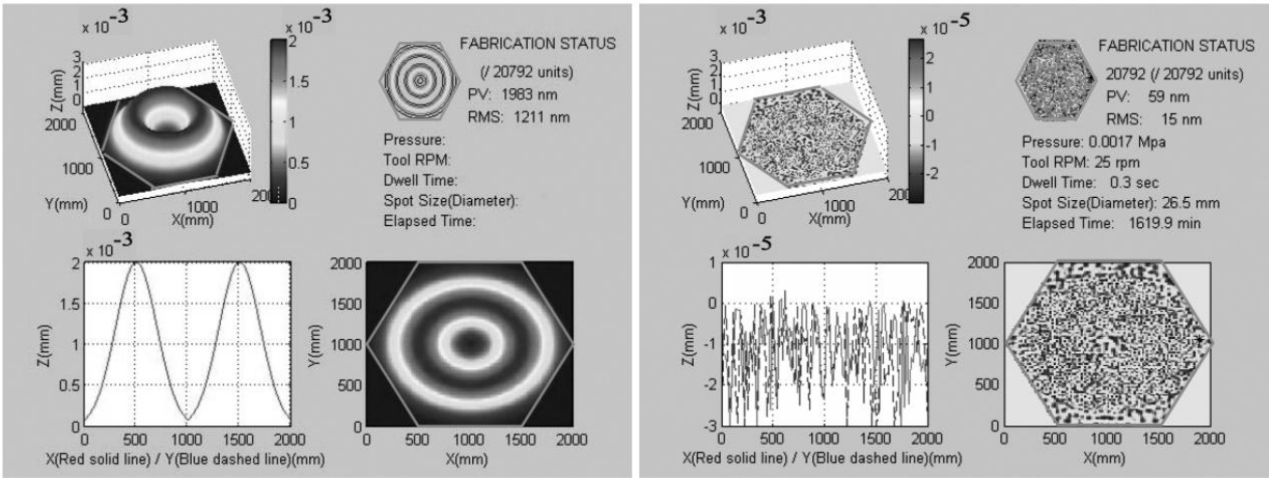

Figure-14. Initial (left) and final (right) surface status for the donut-like case

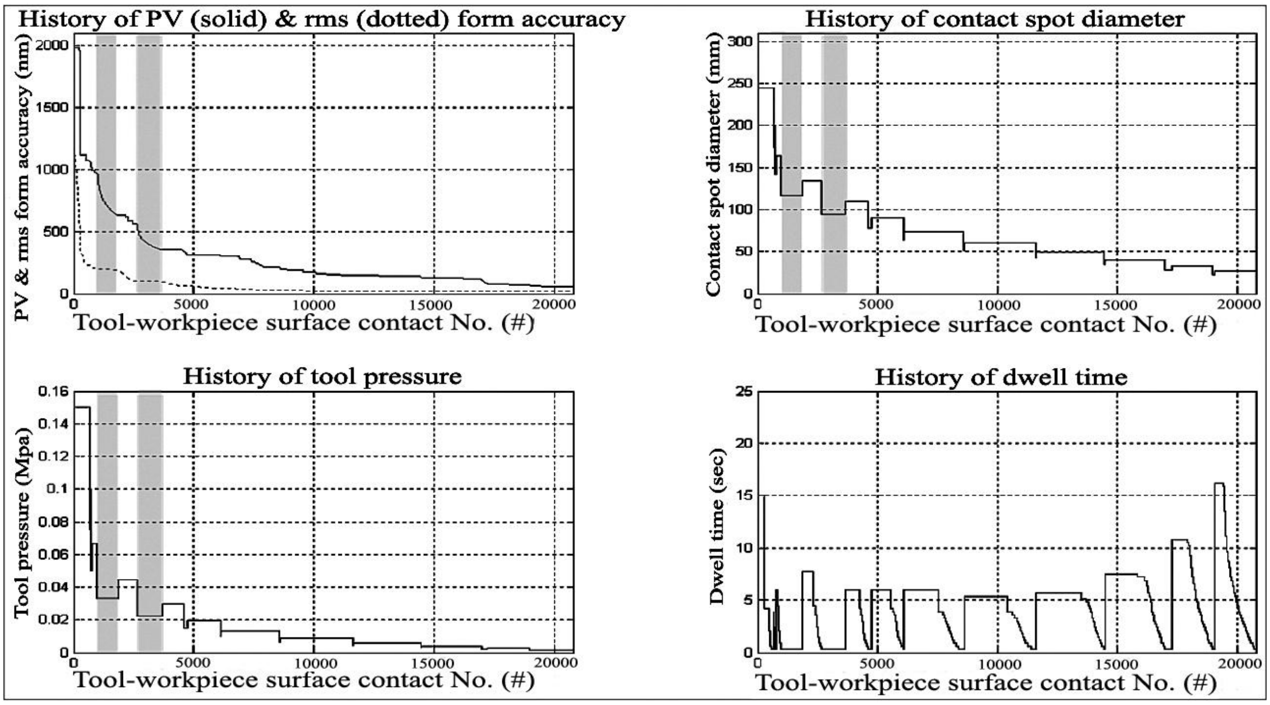

Figure-15. Evolution of control & surface parameters (donut-like case)

4.1.3. Case-III: Circularly non-symmetric donut

The ‘circularly non-symmetric donut’ error was designed to test the true 3-D simulation capability for hexagonal aspheric segments. The X and Y axis error profiles in Figure 16 (left) are different, these being resulted from the combination of donut and saddle surfaces. The initial PV form accuracy was 1.995um that is almost same as the case-I and II. The initial rms was 979nm that is smaller than the case-II. The final PV form accuracy and rms accuracy reached 57nm and 15nm respectively and these figures are almost same as the donut-like case (case-II). We confirmed that the simulation is capable of producing the similar final error figures for both symmetric (case-II) and non-symmetric (case-III) initial form errors, thus proving true 3D fabrication capability.

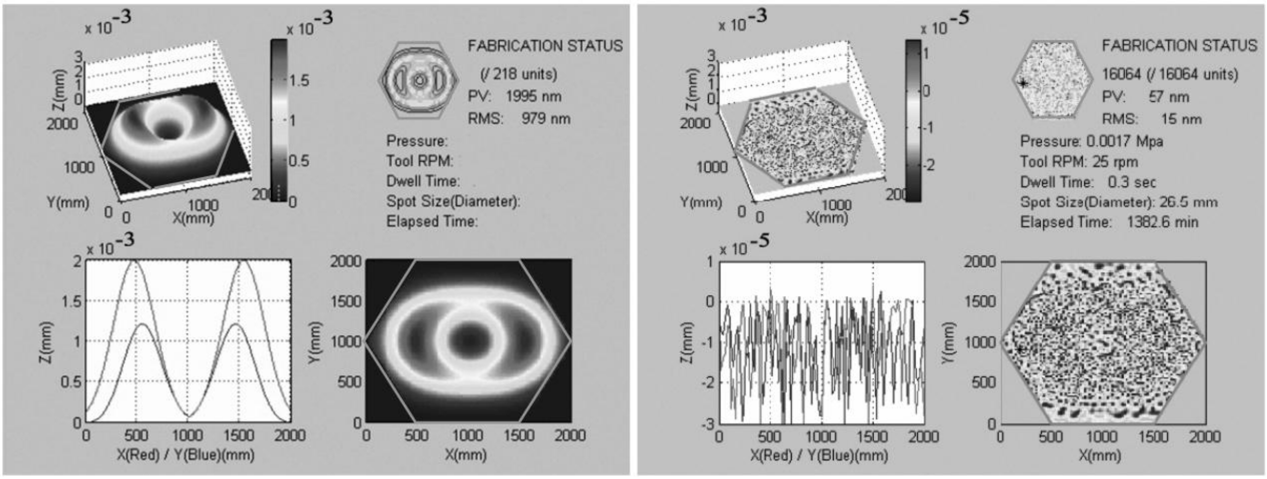

Figure-16. Initial (left) and final (right) surface status for the circularly non-symmetric donut case

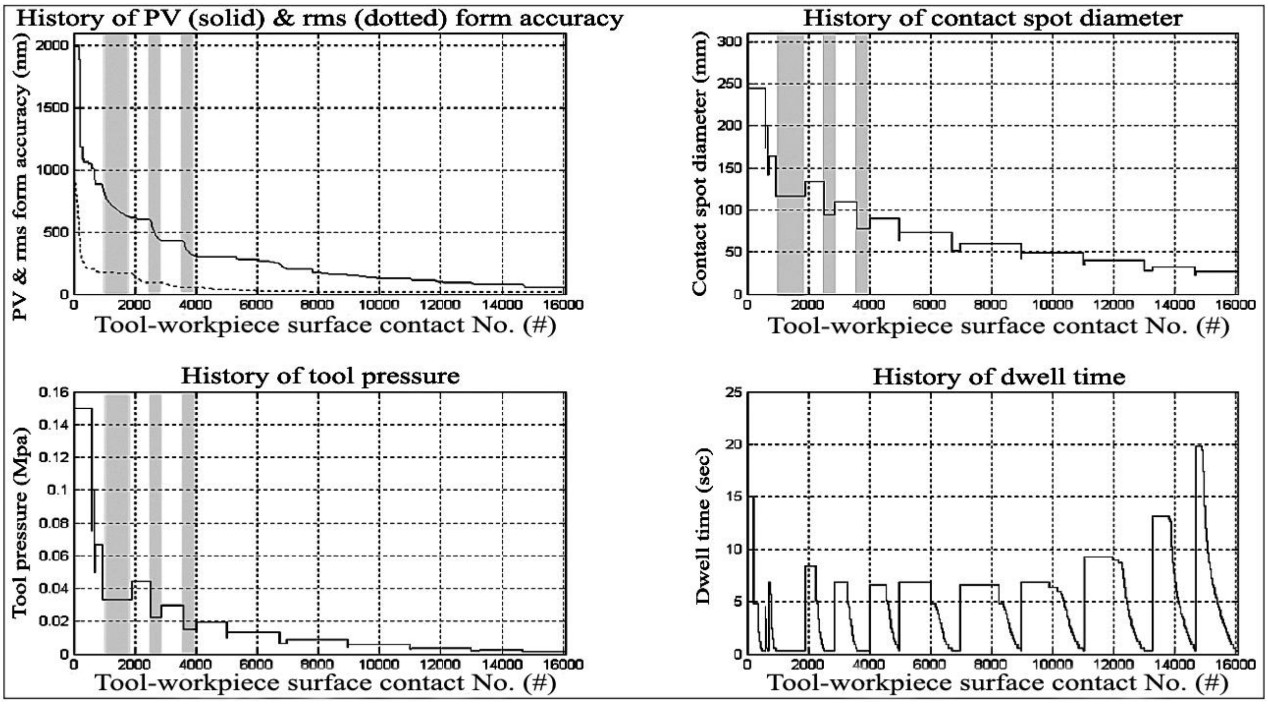

Figure-17. Evolution of control & surface parameters (circularly non-symmetric donut case)

4.2. Summary and implications to mass fabrication of ELT segments

Table-3. Results of the three final simulations: case-I, II, and III

	Case	Shape	Initial form accuracy status		Final form accuracy status		Fabrication status	
			PV (nm)	rms (nm)	PV (nm)	rms (nm)	# of tool-workpiece surface contact: n_{Single_Fab} (#)	Net Fabrication time: t_{Net} (min)
Symmetric	I	Bulged-center	2000	400	49	10	5078	190.4
	II	Donut-like	1983	1211	59	15	20792	1619.9
Asymmetric	III	Circularly non-symmetric donut	1995	979	57	15	16064	1382.6

The comparison of the three simulation results is summarized in Table 3 and shows that the target PV form accuracy of less than 1/10 wave was achieved for all three cases. Using the net fabrication time in Table 3, we can estimate the total fabrication time of ELT segments under a set of reasonable assumptions for the realistic fabrication environment as listed below.

- t_{Tool_Move}: time required for tool stepping motion from one position to the other position
- $t_{Measure}$: time duration for preparation of the next polishing run including surface form measurement
- $n_{Measure}$: number of measuring during the whole fabrication process
- $n_{Machine}$: number of fabrication machine with bulged precessing tool
- n_{Seg}: number of required total segments for an ELT
- r_{Extra_Seg}: ratio of the extra segments to the required total segments
- r_{Risk}: ratio of the delayed time to the total fabrication time without unexpected situations

With these assumptions, the realistic total fabrication time scale t_{Total} for the mass production can be written as below.

$$t_{Total} = [t_{Net} + (n_{Single\_Fab} \cdot t_{Tool\_Move}) + (t_{Measure} \cdot n_{Measure})] \times [\frac{n_{Seg} \cdot (1 + r_{Extra\_Seg})}{n_{Machine}}] \times (1 + r_{Risk}) \qquad (6)$$

, where t_{Net} is the net fabrication time, and n_{Single_Fab} the number of 'tool-workpiece surface contact' in Table 3.

Table-4. Time estimation for the fabrication of EURO50 primary segments

Shape	t_{Net}	n_{Single_Fab}	t_{Tool_Move}	$t_{Measure}$	$n_{Measure}$	n_{Seg}	r_{Extra_Seg}	$n_{Machine}$	r_{Risk}	t_{Total}
	(min)	*(#)*	*(min)*	*(day)*	*(#)*	*(#)*		*(#)*		*(month)*
Bulged-center	190.4	5078	0.5	1	10	618	0.01	20	0.2	15
Donut-like	1619.9	20792	0.5	1	10	618	0.01	20	0.2	23
Circularly non-symmetric donut	1382.6	16064	0.5	1	10	618	0.01	20	0.2	21
Notes	*Table-4*	*Table-4*	*average*			*EURO50*				

With the reasonable assumptions highlighted in the shaded columns, the total fabrication time for the EURO50 primary segments is estimated in Table 4. The total fabrication time, of course, should be linearly decreased as the number of machine is increased. The number of surface measurements was assumed to be 10 during the single mirror fabrication process and the time duration for preparation of the next polishing run including surface form measurement is assumed as 1 day. We can see the fact that the time consumption rate of the measuring process is the most significant factor under this assumption in Figure 18. We allowed for 20% schedule margin to deal with unforeseen incidents, and 1% extra segment units. Summing up the calculation, we estimate that it would take about ~2 years to fabricate 618 units of 2m-class hexagonal conic segments for the EURO50 primary mirror. The surface error dependent fabrication time budget is shown in Figure 18.

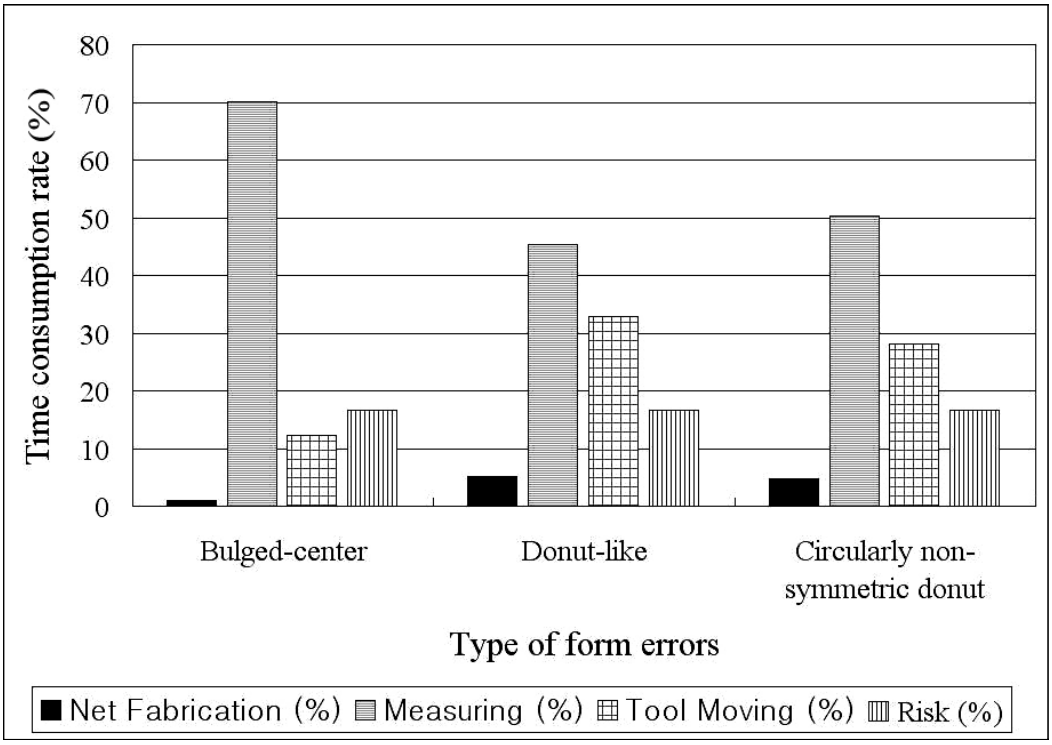

Figure-18. Case dependent fabrication time budget

5. CONCLUDING REMARKS

We developed a new 3D polishing simulation technique for efficient fabrication of 2m class hexagonal segment mirrors with tight specifications. The theoretical background of material removal with the bulged precessing tooling was established in the form of the computer generated TIFs, of which validity was subsequently proved by the measured TIFs[5, 6] for various polishing parameters. These TIFs were then fed into the in-house developed polishing simulator equipped with a number of innovative features including the floating tool trajectory management and machining variable optimization. The fabrication simulation of the 2m hexagonal segment with three difference forms of 2um initial PV form accuracy was then performed, and yielded the final PV form accuracy of 1/10 wave (600nm) and the rms accuracy of around 1/50 wave. These figures are well within the target surface form error specification originally defined for the technology demonstration presented here. Using the first order approximation with a set of reasonable assumptions for the real-time fabrication environments, we estimate the total fabrication time of about 2 years for the 618 units of hexagonal segments of the EURO50 primary mirrors. This new 3D polishing simulation technique presented here forms an important part of the essential technology for prompt materialization of the extremely large telescopes currently in drawing boards world-wide.

ACKNOWLEDGEMENT

We acknowledge the financial support under the Grant code M1-0332-00-0011 from Korea Institute of Machinery and Materials.

REFERENCES

1. T. Andersen, A.L. Ardeberg, J. Beckers, A. Goncharov, M. Owner-Petersen, H. Riewaldt, R. Snel, and D. Walker, "The Euro50 Extremely Large Telescope," *in Future Giant Telescopes*, J.R.P. Angel and R. Gilmozzi, eds., *SPIE* **4840**, pp214-225, 2003.

2. D.D. Walker, A.P. Doel, R.G. Bingham, D. Brooks, A.M. King, G. Peggs, B. Hughes, S. Oldfield, C. Dorn, H. McAndrews, G. Dando, and D. Riley, *Design Study Report: The Primary and Secondary Mirrors for the Proposed Euro50 Telescope*, Chapter-4, University College London, National Physical Laboratory, QinetiQ Ltd, Zeeko Ltd, 2002.

3. P. Dierickx, "Optical fabrication in the large," *in Proceedings of the Backaskog workshop on extremely large telescopes*, T. Andersen, A. Ardeberg, and R. Gilmozzi, eds., ESO conference and workshop proceedings, **no. 57**, pp224, Lund Observatory and European Southern Observatory, Munchen, 2000.

4. T.S. Mast, J.E. Nelson, and G.E. Sommargren, "Primary mirror segment fabrication for CELT," *in Optical Design, Materials, Fabrication, and Maintenance*, P. Dierickx, ed., *Proc. SPIE* **4003**, pp43-58, 2000.

5. D.D. Walker, A.T. Beaucamp, R.G. Bingham, D. Brooks, R. Freeman, S.W. Kim, A. King, G. McCavana, R. Morton, D. Riley, and J. Simms, "Precessions aspheric polishing : - new results from the development programme," *in Optical Manufacturing and Testing V*, H.P. Stahl, ed., *Proc. SPIE* **5180**, pp15-28, 2004.

6. D.D. Walker, D. Brooks, A. King, R. Freeman, R. Morton, G. McCavana, and S.W. Kim, "The 'Precessions' tooling for polishing and figuring flat, spherical and aspheric surfaces", Optics Express, **11**, pp958-964, 2003.

7. D.H. Kim, *On the removal of Material for Polishing Aspheric Optics*, PhD Thesis, Department of physics and Astronomy, University College, London, 2001.

*letter2dwk@hotmail.com; phone 82 – 2 – 2123 – 2688; fax 82 – 2 – 392 – 7680